Applied Surface Science 469 (2019) 747–752

Contents lists available at ScienceDirect

Applied Surface Science

journal homepage: www.elsevier.com/locate/apsusc

Full Length Article

The growth of metastable fcc $Fe_{78}Ni_{22}$ thin films on H-Si(1 0 0) substrates suitable for focused ion beam direct magnetic patterning

Jonas Gloss[a], Michal Horký[b], Viola Křižáková[c], Lukáš Flajšman[b], Michael Schmid[a], Michal Urbánek[b,c,*], Peter Varga[a,b,†]

[a] Institute of Applied Physics, TU Wien, 1040 Vienna, Austria
[b] CEITEC BUT, Brno University of Technology, Purkyňova 123, 612 00 Brno, Czech Republic
[c] Institute of Physical Engineering, Brno University of Technology, Technická 2, 616 69 Brno, Czech Republic

ARTICLE INFO

Keywords:
Magnetic nanostructures
Metastable films
fcc Fe
Cu buffer layer
Si(1 0 0)

ABSTRACT

We have studied the growth of metastable face-centered-cubic, non-magnetic $Fe_{78}Ni_{22}$ thin films on silicon substrates. These films undergo a magnetic (paramagnetic to ferromagnetic) and structural (fcc to bcc) phase transformation upon ion beam irradiation and thus can serve as a material for direct writing of magnetic nanostructures by the focused ion beam. So far, these films were prepared only on single-crystal Cu(1 0 0) substrates. We show that transformable $Fe_{78}Ni_{22}$ thin films can also be prepared on a hydrogen-terminated Si(1 0 0) with a 130-nm-thick Cu(1 0 0) buffer layer. The H-Si(1 0 0) substrates can be prepared by hydrofluoric acid etching or by annealing at 1200 °C followed by adsorption of atomic hydrogen. The Cu(1 0 0) buffer layer and $Fe_{78}Ni_{22}$ fcc metastable thin film were deposited by thermal evaporation in ultra-high vacuum. The films were consequently transformed *in-situ* by 4 keV Ar^+ ion irradiation and *ex-situ* by a 30 keV Ga^+ focused ion beam, and their magnetic properties were studied by magneto-optical Kerr effect magnetometry. The substitution of expensive copper single crystal substrate by standard silicon wafers dramatically expands application possibilities of metastable paramagnetic thin films for focused-ion-beam direct magnetic patterning.

1. Introduction

Magnetic nanopatterning plays a central role in the development of novel devices and magnetic metamaterials with properties unattainable in bulk systems. The patterning is conventionally achieved by using optical or electron-beam lithography in combination with lift-off and etching procedures. However, these methods do not allow, for example, for continuous spatial changes in magnetic properties. The resulting structures usually have sharp magnetic-nonmagnetic transitions leading to, e.g., highly localized demagnetizing fields, or stochastic distribution of pinning sites that cannot be controlled merely by the fabrication process itself. An alternative to the traditional lithography is a fabrication of magnetic elements by ion beams [1]. The ion beam can modify the magnetic properties of a material by alloying [2], intermixing [3] or by a structural change [4]. We have shown that it is possible to embed ferromagnetic body-centered-cubic (bcc) nanostructures in epitaxial paramagnetic face-centered-cubic (fcc) films with an Ar^+ ion beam [4,5]. The system used in these works was fcc Fe grown on a Cu(1 0 0) substrate [6,7]. The ion beam induces a structural and magnetic phase change by overcoming the potential barrier between the fcc local minimum and the bcc global minimum and we, therefore, call these fcc films metastable. The metastable Fe/Cu(1 0 0) spontaneously transforms to the bcc phase at 10 ML [8], but this limit can be shifted to 22 ML by dosing CO [9] and even further by alloying Fe with 22% of Ni [10]. We have shown that it is possible to fabricate magnetic nanostructures in these films by ion-beam irradiation using proximity masks [5] or focused ion beams (FIB) and that by suitably chosen FIB patterning procedures it is possible to tune saturation magnetization and also the magnetic anisotropy of the transformed structures [11].

Metastable $Fe_{78}Ni_{22}$/Cu(1 0 0) is an excellent system for a one-step fabrication of magnetic nanostructures, but the copper single crystal is an expensive substrate for use in future applications. Here we show that it is possible to use also standard Si(1 0 0) wafers as a base substrate for this system. Silicon has been the most commonly used material in the semiconductor industry and scientific research for decades, not only for its electronic properties but also because of the well-known processes for preparation of very well defined substrates with almost perfect

* Corresponding author.
E-mail address: michal.urbanek@ceitec.vutbr.cz (M. Urbánek).
† Deceased 27 October 2018.

https://doi.org/10.1016/j.apsusc.2018.10.263
Received 7 August 2018; Received in revised form 22 October 2018; Accepted 30 October 2018
Available online 31 October 2018

crystallographic properties. Our experiments indicate that the Fe does not grow epitaxially on Si(1 0 0), but it is possible to grow a Cu(1 0 0) buffer layer on Si(1 0 0) [12–14]. The Cu buffer layer grows in the desired (1 0 0) crystallographic orientation when the Si(1 0 0) surface is unreconstructed and hydrogen-terminated (H-Si), which is most commonly achieved by etching in hydrofluoric acid (HF) [12–17]. The lattice constants of Cu and unreconstructed Si lead to a significant (33.5%) lattice mismatch; however, rotation by 45° decreases the lattice mismatch to 6%.

Additionally to the known HF etching procedure, we have also used an ultrahigh vacuum (UHV) alternative, which requires annealing of Si at 1200 °C followed by adsorption of atomic hydrogen. The growth of the 130 nm thick Cu(1 0 0) buffer layer on H-Si substrates prepared by both procedures was tested together with the subsequent deposition of the metastable fcc $Fe_{78}Ni_{22}$ films. The transformation to the bcc phase was performed both, *in-situ* by a weakly focused ion beam and *ex-situ* by the FIB. Measurement of the magnetic properties of the transformed thin films and nanostructures performed by Kerr magnetometry show that $Fe_{78}Ni_{22}$/Cu(1 0 0)/H-Si(1 0 0) is a viable alternative to systems prepared on Cu(1 0 0) single-crystal substrates.

2. Experimental

The UHV system used for the experiments has a base pressure of 7×10^{-11} mbar (measured by a Bayard-Alpert ionization gauge) and is equipped with a three-pocket e-beam evaporator (Focus EFM3T), a single-pocket e-beam evaporator (Focus EFM3) and a Knudsen effusion cell (CreaTec). The samples can be cooled by liquid nitrogen to 100 K and heated by e-beam bombardment of the sample holder plate to 1000 K. Auger electron spectroscopy (AES) was used to check the cleanliness of the substrates and the composition of grown films. The AES spectra have been normalized to the minimum of the average peak-to-peak height of the dominant peak. The concentrations reported in this paper correspond to quantitative analysis using relative elemental sensitivity factors [18]. The structure of the surfaces was measured by Low energy electron diffraction (LEED). The LEED images were post-processed with a dark-field subtraction, flat-field normalization [19] and inverted.

The experiments were performed on B-doped (p-type) Si with a resistivity of 5–20 Ωcm. The dimensions of the samples were $3 \times 12 \times 0.4\,mm^3$. Two procedures were applied to obtaining a H-terminated surface. The chemically treated Si was etched for 2.5 min in 10% HF to remove the native oxide and to terminate the Si with hydrogen [17], then rinsed for 1 min in high-purity (Merck Milli-Q) water, dried with argon gas and transferred into a loadlock connected to the UHV chamber within 10 min after etching. The H-terminated Si should be inert to the ambient atmosphere for such a period [17]. Then, the sample was outgassed in the UHV chamber at 100 °C for 30 min. After this procedure, the sample cleanliness was checked by AES and the surface reconstruction by LEED.

In the UHV procedure, Si samples were heated by direct current (DC) heating in a home-built heating stage. Target holders were made of Mo; their design was based on the Omicron sample plates for DC heating. After introducing the samples into UHV, we outgassed the sample holder by heating it to 600 °C for approx. 20 h. We then heated the samples by DC to 600 °C for approx. 20 h until the base pressure in the chamber was restored. After the outgassing phase, we annealed the samples repeatedly at 1200 °C by DC for 5 s with a 5-second ramp from the outgassing temperature. The highest pressure during the last annealing step was kept below 5×10^{-10} mbar. With this approach, we were able to completely remove both the native oxide and also any organic impurities. The H termination was achieved by a home-built H-cracker based on the design of Bischler [20]. A tungsten capillary with a 0.6 mm inner diameter was heated by 1 keV e-beam bombardment to approx. 1800 °C, which completely dissociated the H_2 flowing through it [21]. The end of the capillary was approx. 3 cm from the sample and a liquid-N_2-cooled Cu plate between the W tube and the sample limited the sample heating to approx. 1 °C/min. The sample was exposed to atomic hydrogen (1×10^{-6} mbar H_2 backpressure) for 7 mins to achieve a complete H termination. Again, the sample cleanliness was checked by AES and the surface reconstruction by LEED.

Cu was evaporated from two sources, the EFM3, and the effusion cell. The material of the effusion cell crucible contained a small amount of Ca contamination (confirmed by Secondary Ion Mass Spectrometry) which was detectable also in the deposited layer and which turned out to be an essential surfactant needed to stabilize the growth of the Cu buffer layer in the required (1 0 0) orientation on UHV treated samples. The temperature of the sample increased by 10 °C via radiation heating during the deposition from the effusion cell. The pressure during the deposition was 1×10^{-10} mbar (with the help of a liquid-N_2-cooled cryo baffle and a titanium sublimation pump). Deposition rates were calibrated with a quartz crystal microbalance at the position of the substrate, and the deposition was done at room temperature (RT) unless mentioned otherwise. The deposition rate of both Cu evaporators was $0.06\,Å s^{-1}$ (approx. 5.8 h for 130 nm). The $Fe_{78}Ni_{22}$ layers were evaporated by the EFM3T from a rod with a 2 mm diameter (MaTecK). A repelling voltage of +1.5 kV was applied to a cylindrical electrode (flux monitor) in the orifice of the evaporator to suppress high-energy ions, which may modify the growth mode of the films [22]. The base pressure during the deposition was 8×10^{-11} mbar, which was artificially increased to 5×10^{-10} mbar of CO to stabilize the fcc phase in line with previous observations [10]. The deposition rate of $Fe_{78}Ni_{22}$ was $0.02\,Å s^{-1}$ (approx. 1 h for 8 nm). After each deposition step, the surface composition and the crystallographic structure were measured by AES and by LEED, respectively.

Large-Area irradiation of one set of samples was performed *in situ* by an ion gun (Specs) equipped with a Wien filter by scanning the sample with a time-averaged ion flux of approx. $10^{13}\,cm^{-2}s^{-1}$. To maximize the transformation rate, we used 4 keV Ar^+ ions, which penetrate the whole $Fe_{78}Ni_{22}$ layer at perpendicular incidence and do not cause significant Fe-Cu intermixing [23]. During the ion beam irradiation, we periodically measured magnetic hysteresis loops by a home-built surface magneto-optical Kerr effect (SMOKE) apparatus. The SMOKE experiment can be performed in longitudinal or polar geometry (angle of incidence 60° or 30°, respectively, with a spot size of approx. 1 mm). The plane of incidence and the direction of the magnetic field were parallel to the (0 1 0) plane of the Si substrate.

To study the potential of the metastable films for magnetic micro- and nanopatterning, we performed a local ion-beam-induced transformation in a high vacuum (approx. 10^{-7} mbar) chamber of a focused ion beam – scanning electron microscope (FIB-SEM) system (Tescan LYRA3). A series of $3 \times 3\,\mu m^2$ squares was irradiated with the Ga^+ FIB at 30 keV with a spot size of 20 nm and a beam current of 40 pA with an increasing ion dose. We varied the irradiation dose between individual areas and then imaged the patterns by SEM, and analyzed their magnetic response by micro Kerr magnetometry either in a Kerr microscope or in our home-built micro-focused Kerr magnetometer [24].

3. Results and discussion

3.1. Surface structure and stoichiometry

The chemically prepared Si(1 0 0) samples had a (1 × 1) diffraction pattern after introduction into the UHV and mild annealing, which is shown by a green square in Fig. 1a). The unetched, UHV treated Si (1 0 0) showed (2 × 1)-reconstructed domains after annealing to 1200 °C [blue rectangles in Fig. 1(d)] which changed into a (1 × 1) after termination with atomic H [green square in Fig. 1(e)]. The change in reconstruction confirms that the atomic H had saturated all the Si dangling bonds [25,26]. The (1 × 1) diffraction pattern, therefore, means that both approaches are potentially suitable for the growth of epitaxial Cu(1 0 0).

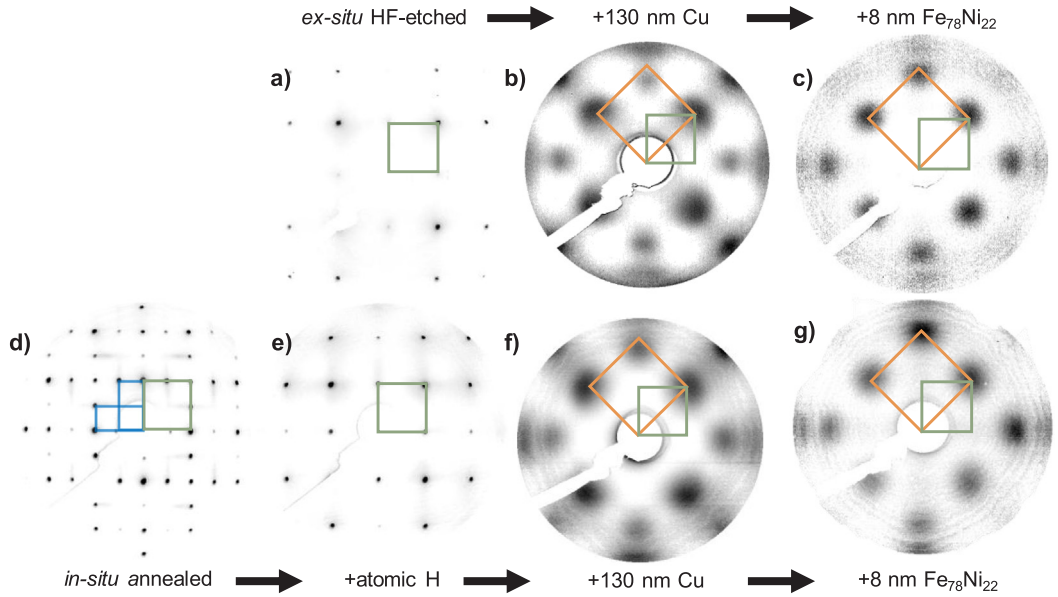

Fig. 1. LEED images taken at 130 eV except for (c) and (g) which were taken at 120 eV. (a) H-Si(1 0 0) with its (1 × 1) unit cell (green in all images) prepared chemically. (b) 130 nm Cu/H-Si(1 0 0) with its (1 × 1) unit cell (orange in all images). (c) 8 nm $Fe_{78}Ni_{22}$/130 nm Cu/H-Si(1 0 0) with its fcc (1 0 0)-(1 × 1) unit cell. (d) UHV-treated Si; blue rectangles are the (2 × 1) reconstruction, which changes into the (1 × 1) after H-termination, shown in (e). LEED patterns (f) and (g) correspond to the deposition steps (b) and (c) on the UHV-treated substrate.

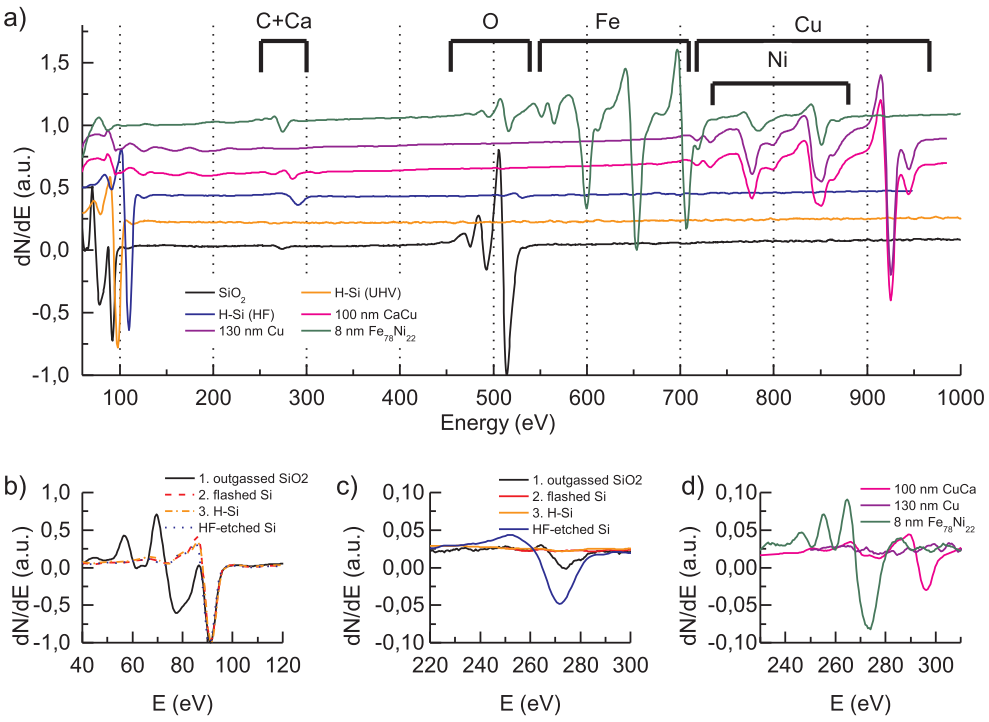

Fig. 2. (a) Overview AES of the cleaning (black, orange and blue lines) and deposition (magenta, violet and green lines) steps. The details in (b) and (c) portray the Si and C peak, respectively. The in-situ-treated Si was outgassed (black), annealed (red) and H-terminated (orange). The blue line corresponds to chemically treated (HF-etched) Si. AES in (d) marks the details of C and Ca peaks measured after the deposition of Ca-containing Cu (magenta), Cu (violet) and $Fe_{78}Ni_{22}$ (green), respectively.

The AES measurement shows that the HF-etched surface after mild annealing (100 °C) contains 15% of C and 2% of O [blue line in Fig. 2(a) and (c)]. Because etching in HF for 2.5 min completely removes the SiO_2, we contribute this signal to imperfect H termination of Si and contamination during transport in the ambient atmosphere before introducing the sample into the UHV. These impurities did not desorb during the mild annealing. Multiple steps of cleaning before the last HF etch can minimize this contamination [17,27]. Excessive contamination of the etched Si can prevent the growth of an epitaxial Cu(1 0 0) buffer layer; Cu then grows in (1 1 1) orientation [28]. H-Si prepared in UHV is much cleaner than the chemically treated Si [compare the orange and blue lines in Fig. 2(a) and (c)]. The outgassed Si with a native SiO_2 is still slightly contaminated by C (black lines in Fig. 2), and after annealing, we observe a complete removal of the native oxide and carbon contamination [compare black and red lines in Fig. 2(c)]. The H termination does not introduce any impurities (orange lines in Fig. 2).

We deposited Cu on both H-Si(1 0 0) substrates prepared chemically and in UHV. We grew 130 nm thick films because at this thickness we found a right balance between the film morphology [13] and the deposition time, which was below 6 h with our evaporators. The LEED patterns after deposition of Cu confirm that the Cu film on the chemically treated substrate was very similar to the one on the H-Si prepared in UHV [Fig. 1(b) and (f)]. Both films showed a 45° rotation of their unit cell with respect to the underlying substrate and a unit cell reduced by a

factor of √2 [marked by orange and green squares in Fig. 1(b) and f)]. The fcc (1 0 0) diffraction spots are diffused, and we could also observe their splitting. Both the diffusive appearance and splitting of the diffraction spots lead to a conclusion that the Cu grows as epitaxial islands with terraces only a few nm wide, as already shown by Mewes et al. [14]. Deposition assisted with ion bombardment from the sputter gun did not yield any significant difference in the as-grown films. Deposition at lower or higher temperatures (−20 °C, > 50 °C) led to a growth of a polycrystalline fcc (1 1 1) film, in line with previous observations [29,30]. Post-annealing did not lead to flattening of the film; in fact, we could observe a signal from Si in AES while heating to 150 °C for two hours, in contrast to Lukaszew et al. [31]. The Si signal in AES after post-anneal showed a splitting in energy, which indicates the formation of bulk copper silicides, i.e., hybridization between the Si 3p states and the Cu 3d states [16].

The 130 nm Cu buffer layer on the chemically prepared H-Si was completely clean according to AES [violet lines in Fig. 2(a) and (d)], indicating that the impurities had either desorbed or got buried by Cu deposition. We were not able to deposit an fcc (1 0 0) Cu buffer layer on the UHV prepared H-Si by depositing pure Cu, but we were successful when we used a Ca-containing Mo crucible in the effusion cell. The surface of the 100 nm Cu films deposited from the Ca-containing Mo crucible showed a Ca concentration of 2%. This is not necessarily the concentration in the films; Ca is virtually insoluble in Cu [32], so it is likely that Ca floats to the top during the growth and only a negligible part is incorporated. Ca has an fcc structure and a 2.8% lattice mismatch to Si(1 0 0) and in this case, it most probably served as a surfactant supporting the epitaxial growth. After deposition of 100 nm fcc (1 0 0) Cu [magenta lines in Fig. 2(a) and (d)], we have continued with deposition of 30 nm of pure Cu, and AES measurements after the deposition [identical with the violet lines in Fig. 2 (a) and (d)] revealed that the completed film does not have any Ca on the surface.

In the last step of the film preparation, we deposited 8 nm of $Fe_{78}Ni_{22}$(1 0 0) on the epitaxial Cu(1 0 0) buffer layer grown on both substrates. The diffraction spots in Fig. 1(c) and (g) are commensurate, not split and similarly diffuse as the ones of the Cu buffer layer [Fig. 1(b) and (f)]. The spot shape indicates that the $Fe_{78}Ni_{22}$ and the buffer layers beneath have similar morphology and that the structure of the metastable film is also fcc (1 0 0). As the films were deposited with a CO background pressure, the surface of the metastable films had 8% C and 5% O measured by AES, as shown by the green line in Fig. 2(a) and by the detail of the C-peak in Fig. 2(d). The C and O peaks arise from the dissociation of the CO in which the films are deposited, as described elsewhere [9]. The combination of LEED and AES demonstrates that it is possible to grow epitaxial films of $Fe_{78}Ni_{22}$(1 0 0) on H-Si(1 0 0) prepared by wet chemistry or in UHV.

3.2. In-situ magnetic transformation by broad-beam irradiation

The experiments presented in Figs. 3 and 4 were performed on samples prepared by the UHV treatment; the samples treated by wet chemistry showed equivalent results. SMOKE measurements of the as-deposited films [black circles in Fig. 3(a)] show a non-zero magnetic signal suggesting a very small fraction of the film is already in the bcc ferromagnetic (FM) phase. Irradiation with a dose of 2×10^{15} cm^{-2} leads to partial magnetic transformation; the hysteresis loop [green line in Fig. 3(a)] exhibits high coercivity and the Kerr signal reaches approx. 50% of the maximum value measured for the fully transformed film. The film is completely transformed upon applying a transformation dose of 6×10^{15} cm^{-2} [red squares in Fig. 3(a)].

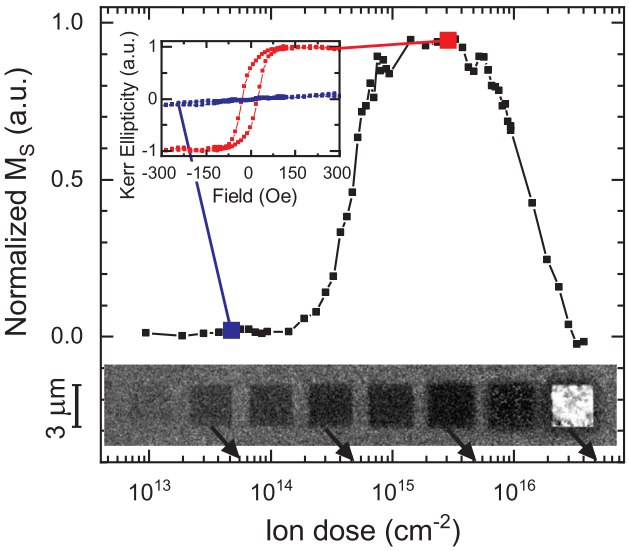

Fig. 4. SEM and Kerr magnetometry analysis of 3 × 3 µm^2 squares in the 8-nm $Fe_{78}Ni_{22}$/130 nm Cu/Si(1 0 0) film irradiated by a 30 keV Ga^+ FIB for different ion doses. The Kerr magnetometry confirms that there is no ferromagnetic signal in films irradiated with doses below 5×10^{13} cm^{-2} (blue line in the top-left inset). The film has largest magnetic saturation (M_S) when irradiated by 3×10^{15} cm^{-2} (red line in the top left inset). The surrounding fcc material does not show any hysteresis. The inset at the bottom shows SEM images of the irradiated squares for the ion doses at the abscissa (with half-decade steps starting at 1×10^{13} cm^{-2}).

We demonstrate the development of the magnetic transformation with increasing ion dose by the magenta line in Fig. 3(b). We do not detect any increase of the magnetization up to the ion dose of 2×10^{14} cm^{-2}. The magnetic signal then increases with the increasing ion dose up to a dose of 6×10^{15} cm^{-2}, where it reaches a maximum and then decreases as the magnetic thin film is sputtered away and intermixes with the Cu layer below. The ion dose at which we reach the maximum transformation is equal to the transformation dose for films grown on a Cu(1 0 0) single crystal [10]. The Kerr ellipticity of the transformed film is 10% lower than in the case of the films deposited on a Cu(1 0 0) single crystal [10], which we attribute to the corrugation of the metastable film arising from the underlying Cu buffer layer.

The coercivity [blue line in Fig. 3(b)] starts increasing at the same ion dose as the magnetization (around 2×10^{14} cm^{-2}) and reaches a maximum at 2×10^{15} cm^{-2}. It then falls rapidly to its minimum, which matches the maximum of the magnetic saturation at 6×10^{15} cm^{-2}.

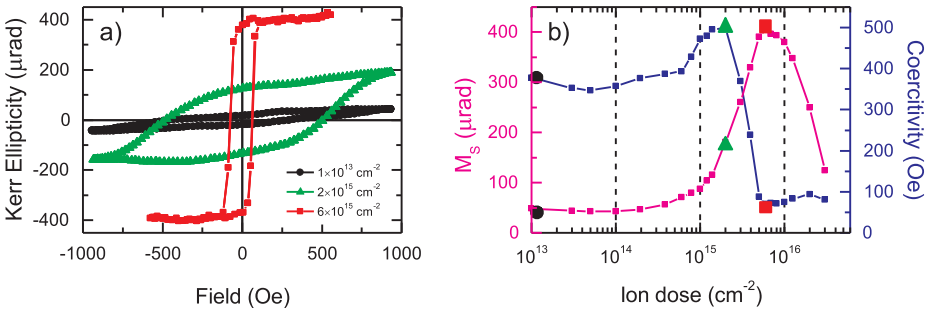

Fig. 3. SMOKE measurements of a metastable 8 nm $Fe_{78}Ni_{22}$ film on 130 nm Cu/H-Si(1 0 0). (a) the as-deposited film is weakly FM (black). The film partially transforms to bcc (green) after irradiation with dose of 2×10^{15} cm^{-2}. The magnetization reaches a maximum at an ion dose 6×10^{15} cm^{-2} (red). (b) dependence of the Kerr ellipticity at magnetic saturation (M_S, magenta) and coercivity (blue) on the ion dose. Black, green and red symbols correspond to the measurements in (a).

From observations on a Cu(1 0 0) single-crystal substrate we know that increasing the ion dose increases the number and size of bcc nuclei randomly dispersed in the fcc layer. The maximum in the coercive field corresponds to the nuclei reaching the maximum size for single magnetic domains. This property is well known from magnetic nanoparticle studies [33]. Further lowering of the coercive field is attributed to multi-domain states of magnetic particles and more efficient interaction in between the nanoparticles through the stray field of individual particles.

3.3. Focused ion beam magnetic patterning

Fig. 4 shows the results of patterning the metastable films with the FIB. The grey level in SEM (inset at the bottom of Fig. 4) allows for distinguishing the as-deposited (grey) areas and the irradiated (darker or brighter) areas and serves as a valuable pre-characterization tool. The irradiated areas become darker at a dose of 5×10^{13} cm^{-2} but brighten again at doses above 10^{16} cm^{-2}. The reason for the decrease of the SEM signal is the fcc → bcc structural change, which affects electron channeling and associated secondary electron emission [11]. The last square then shows the signal from the Cu buffer layer after a complete removal of the $Fe_{78}Ni_{22}$ film.

The data from Kerr magnetometry (Fig. 4) show the onset of the magnetic transformation at an ion dose of 2×10^{14} cm^{-2}. The maximum of the magnetization is achieved at ion doses of 1×10^{15} cm^{-2}–3×10^{15} cm^{-2}. The transformation by 30 keV Ga^+ ions qualitatively shows the same behavior as the transformation performed *in-situ* [see Fig. 3(b)], but the ion dose needed to achieve full transformation is two times lower for the Ga^+. According to SRIM [23], the the energy deposited into FeNi by 4 keV Ar^+ ion is 4 keV and by 30 keV Ga^+ ion is on average 20.4 keV. This explains the higher efficiency of the transformation by 30 keV Ga^+ compared to 4 keV Ar^+, despite the fact that 64% of the 30 keV Ga^+ ions pass through the FeNi and stop in the Cu layer.

The inset in Fig. 4 shows the hysteresis loops of the squares irradiated by a very low ion dose (blue) and at the maximum magnetization (red line). The squares irradiated by a very low ion dose do not show any FM signal, which is in contrast with the measurement by SMOKE in Fig. 3 (black line). We assume this is because the SMOKE collects signal from a large area, and the small fraction of the film which is already in the bcc ferromagnetic (FM) phase is not recognizable by the micro-Kerr magnetometer.

4. Conclusion

We have shown that it is possible to grow metastable, epitaxial fcc $Fe_{78}Ni_{22}$ on H-Si(1 0 0) with a Cu(1 0 0) buffer layer, and that using a focused ion beam, we can create magnetic micro- and nanostructures with tuneable magnetization. The lower size limit of such nanostructures is given by the focus of the ion beam and the size of the bcc nuclei [5]. The magnetic properties of the films are comparable to the properties of $Fe_{78}Ni_{22}$ films prepared on Cu(1 0 0) single-crystal substrates [11]. We have presented two (UHV and chemical) possibilities for the preparation of the H-Si(1 0 0) substrate of which the UHV alternative has not been used in the past. We have stabilized the Cu(1 0 0) buffer layer on the UHV prepared H-Si(1 0 0) by addition of Ca. Future research should focus on creating a flat Cu(1 0 0) buffer layer by, e.g., introducing a wetting layer. Also, the role of Ca in the stabilization of the epitaxial growth of Cu(1 0 0) warrants further investigations.

Metastable films for ion-beam-induced magnetic transformation present a promising system for fabrication of magnetic metamaterials, such as magnonic crystals. They are an alternative to standard lithography approaches, and the possibility to use a standard substrate such as Si(1 0 0) is undoubtedly an essential step towards applications in rapid prototyping of magnetic metamaterials (by using FIB) and in suitability for mass production (by ion irradiation through a mask).

Acknowledgments

This research has been financially supported by the joint project of Grant Agency of the Czech Republic (Project No. 15-34632L) and Austrian Science Fund (Project No. I 1937-N20) and by the CEITEC Nano + project (ID CZ.02.1.01/0.0/0.0/16013/0001728). Part of the work was carried out in CEITEC Nano Research Infrastructure (ID LM2015041, MEYS CR, 2016–2019). L.F. was supported by Brno PhD talent scholarship, and V.K. was supported by Thermo Fischer Scientific student scholarship.

References

[1] C. Chappert, H. Bernas, J. Ferre, V. Kottler, J.P. Jamet, Y. Chen, E. Cambril, T. Devolder, F. Rousseaux, V. Mathet, H. Launois, Planar patterned magnetic media obtained by ion irradiation, Science 280 (1998) 1919–1922, https://doi.org/10.1126/science.280.5371.1919.

[2] M.T. Georgieva, P.J. Grundy, N.D. Telling, Ion irradiation and thermally induced mixing of CoCrPt/Cr multilayered films, Appl. Phys. Lett. 90 (2007) 042509, https://doi.org/10.1063/1.2432256.

[3] E. Menendez, M.O. Liedke, J. Fassbender, T. Gemming, A. Weber, L.J. Heyderman, K.V. Rao, S.C. Deevi, S. Surinach, M.D. Baro, J. Sort, J. Nogues, Direct magnetic patterning due to the generation of ferromagnetism by selective ion irradiation of paramagnetic FeAl alloys, Small 5 (2009) 229–234, https://doi.org/10.1002/smll.200800783.

[4] W. Rupp, A. Biedermann, B. Kamenik, R. Ritter, C. Klein, E. Platzgummer, M. Schmid, P. Varga, Ion-beam induced fcc-bcc transition in ultrathin Fe films for ferromagnetic patterning, Appl. Phys. Lett. 93 (2008) 063102, https://doi.org/10.1063/1.2969795.

[5] S. Shah Zaman, P. Dvořák, R. Ritter, A. Buchsbaum, D. Stickler, H.P. Oepen, M. Schmid, P. Varga, In-situ magnetic nano-patterning of Fe films grown on Cu (100), J. Appl. Phys. 110 (2011) 024309, https://doi.org/10.1063/1.3609078.

[6] A. Biedermann, M. Schmid, P. Varga, Nucleation of bcc iron in ultrathin fcc films, Phys. Rev. Lett. 86 (2001) 464–467, https://doi.org/10.1103/PhysRevLett. 86.464.

[7] A. Biedermann, R. Tscheliessnig, M. Schmid, P. Varga, Crystallographic structure of ultrathin Fe films on Cu(100), Phys. Rev. Lett. 87 (2001) 086103, https://doi.org/10.1103/PhysRevLett. 87.086103.

[8] J. Thomassen, F. May, B. Feldmann, M. Wuttig, H. Ibach, Magnetic live surface layers in Fe/Cu(100), Phys. Rev. Lett. 69 (1992) 3831–3834, https://doi.org/10.1103/PhysRevLett. 69.3831.

[9] A. Kirilyuk, J. Giergiel, J. Shen, M. Straub, J. Kirschner, Growth of stabilized gamma-Fe films and their magnetic properties, Phys. Rev. B 54 (1996) 1050–1063, https://doi.org/10.1103/PhysRevB.54.1050.

[10] J. Gloss, S. Shah Zaman, J. Jonner, Z. Novotny, M. Schmid, P. Varga, M. Urbánek, Ion-beam-induced magnetic and structural phase transformation of Ni-stabilized face-centered-cubic Fe films on Cu(100), Appl. Phys. Lett. 103 (2013) 262405, https://doi.org/10.1063/1.4856775.

[11] M. Urbánek, L. Flajšman, V. Křižáková, J. Gloss, M. Horký, M. Schmid, P. Varga, Research update: Focused ion beam direct writing of magnetic patterns with controlled structural and magnetic properties, APL Materials 6 (2018) 060701, https://doi.org/10.1063/1.5029367.

[12] C.-A. Chang, Outdiffusion of Cu through Au: Comparison of (100) and (111) Cu films epitaxially deposited on Si, and effects of annealing ambients, Appl. Phys. Lett. 55 (1989) 2754–2756, https://doi.org/10.1063/1.101944.

[13] A. Meunier, B. Gilles, M. Verdier, Cu/Si(001) epitaxial growth: role of the epitaxial silicide formation in the structure and the morphology, J. Cryst. Growth 275 (2005) e1059–e1065, https://doi.org/10.1016/j.jcrysgro.2004.11.132.

[14] T. Mewes, M. Rickart, A. Mougin, S.O. Demokritov, J. Fassbender, B. Hillebrands, M. Scheib, Comparative study of the epitaxial growth of Cu on MgO(001) and on hydrogen terminated Si(001), Surf. Sci. 481 (2001) 87–96, https://doi.org/10.1016/S0039-6028(01)01000-7.

[15] C.-A. Chang, Formation of copper silicides from Cu(100)/Si(100) and Cu(111)/Si (111) structures, J. Appl. Phys. 67 (1990) 566–569, https://doi.org/10.1063/1.345194.

[16] C.A.F. Vaz, S.J. Steinmuller, C. Moutafis, J.A.C. Bland, A.Y. Babkevich, Structural and morphological characterisation of hybrid Cu/Si(001) structures, Surf. Sci. 601 (2007) 1377–1383, https://doi.org/10.1016/j.susc.2007.01.001.

[17] T. Takahagi, I. Nagai, A. Ishitani, H. Kuroda, Y. Nagasawa, The formation of hydrogen passivated silicon single-crystal surfaces using ultraviolet cleaning and HF etching, J.Appl. Phys. 64 (1988) 3516–3521, https://doi.org/10.1063/1.341489.

[18] L.E. Davis, Handbook of Auger electron spectroscopy: a reference book standard data for identification and interpretation of Auger electron spectroscopy, Phys. Electron. Industr. (1976).

[19] R. Koller, W. Bergermayer, G. Kresse, C. Konvicka, M. Schmid, J. Redinger, R. Podloucky, P. Varga, The structure of the oxygen-induced c(6 x 2) reconstruction of V(110), Surf. Sci. 512 (2002) 16–28, https://doi.org/10.1016/S0039-6028(02)01722-3.

[20] U. Bischler, E. Bertel, Simple source of atomic hydrogen for ultrahigh-vacuum applications, J. Vac. Sci. Technol. A 11 (1993) 458–460, https://doi.org/10.1116/1.578754.

[21] C. Eibl, G. Lackner, A. Winkler, Quantitative characterization of a highly effective atomic hydrogen doser, J. Vac. Sci. Technol. A 16 (1998) 2979–2989, https://doi.

org/10.1116/1.581449.
[22] C. Nagl, O. Haller, E. Platzgummer, M. Schmid, P. Varga, Submonolayer growth of Pb on Cu(111): surface alloying and de-alloying, Surf. Sci. 321 (1994) 237–248, https://doi.org/10.1016/0039-6028(94)90189-9.
[23] J.F. Ziegler, J.P. Biersack, M.D. Ziegler, TRIM, computer code to calculate the stopping and range of ions in matter, found at www.srim.org, (2008).
[24] L. Flajšman, M. Urbánek, V. Křižáková, M. Vaňatka, I. Turčan, T. Šikola, High-resolution fully vectorial scanning Kerr magnetometer, Rev. Sci. Instr. 87 (2016) 053704, https://doi.org/10.1063/1.4948595.
[25] K. Oura, V.G. Lifshits, A.A. Saranin, A.V. Zotov, M. Katayama, Hydrogen interaction with clean and modified silicon surfaces, Surf. Sci. Rep. 35 (1999) 1–69, https://doi.org/10.1016/s0167-5729(99)00005-9.
[26] J.J. Boland, Structure of the H-saturated Si(100) surface, Phys. Rev. Lett. 65 (1990) 3325–3328, https://doi.org/10.1103/PhysRevLett. 65.3325.
[27] B.G. Demczyk, F. Naik, G. Auner, C. Kota, U. Rao, Growth of Cu films on hydrogen terminated Si(100) and Si(111) surfaces, J. Appl. Phys. 75 (1993) 1956–1961, https://doi.org/10.1063/1.356344.
[28] I. Hashim, B. Park, H.A. Atwater, Epitaxial growth of Cu (001) on Si (001): mechanisms of orientation development and defect morphology, Appl. Phys. Lett. 63 (1993) 2833, https://doi.org/10.1063/1.110302.
[29] R. Mansell, D.C.M.C. Petit, A. Fernández-Pacheco, R. Lavrijsen, J.H. Lee, R.P. Cowburn, Magnetic properties and interlayer coupling of epitaxial Co/Cu films on Si, J. Appl. Phys. 116 (2014) 063906, https://doi.org/10.1063/1.4893306.
[30] E.T. Krastev, L.D. Voice, R.G. Tobin, Surface morphology and electric conductivity of epitaxial Cu(100) films grown on H-terminated Si(100), J. Appl. Phys. 79 (1996) 6885, https://doi.org/10.1063/1.361508.
[31] R.A. Lukaszew, Y. Sheng, C. Uher, R. Clarke, Smoothening of Cu films grown on Si (001), Appl. Phys. Lett. 76 (2000) 724, https://doi.org/10.1063/1.125874.
[32] Laughlin Chakrabarti, The Ca-Cu (Calcium-Copper) system, Bull. Alloy Phase Diagr. 5 (1984) 570, https://doi.org/10.1007/BF02868318.
[33] Q. Li, C.W. Kartikowati, S. Horie, T. Ogi, T. Iwaki, K. Okuyama, Correlation between particle size/domain structure and magnetic properties of highly crystalline Fe_3O_4 nanoparticles, Sci. Rep. 7 (2017) 9894, https://doi.org/10.1038/s41598-017-09897-5.